Electronic Structure, Ion Diffusion and Cation Doping in the Na$_4$VO(PO$_4$)$_2$ Compound as a Cathode Material for Na-ion Batteries

Pablo A. Aparicio[a,*] and Nora H. de Leeuw[a,b*]

[a] *School of Chemistry, Cardiff University, Main Building Park Place, Cardiff CF10 3AT, United Kingdom*

[b] *School of Chemistry, University of Leeds, Leeds LS2 9JT, United Kingdom*

Email:
*apariciosanchezp@cardiff.ac.uk
*n.h.deleeuw@leeds.ac.uk

Abstract

Sodium-ion batteries are considered one of the most promising alternatives to lithium-ion batteries owing to the low cost and wide abundance of sodium. Phosphate compounds are promising materials for sodium-ion batteries because of their high structural stability, energy densities and capacities. Vanadium phosphates have shown high energy densities, but their sodium-ion diffusion and cation doping properties are not fully rationalized. In this work, we combine density functional theory calculations and molecular dynamics simulations to study the electronic structure, ion diffusion and cation doping properties of the Na$_4$VO(PO$_4$)$_2$ compound. The calculated Na-ion activation energy of this compound is 0.49 eV, which is typical for Na-based cathode materials, and the simulations predict a Na-ion diffusion coefficient of 5.1×10^{-11} cm^2 s^{-1}. The cell voltage trends show a voltage of 3.3 V *vs.* Na/Na$^+$. Partial substitution of vanadium atoms by other metals (Al^{3+}, Co^{2+}, Fe^{3+}, Mn^{4+}, Ni^{2+} or Ti^{4+}) increases the cell voltage up to 1.1 V *vs.* Na/Na$^+$. These new insights will help us to understand the ion transport and electrochemical behaviour of potential phosphate cathode materials for sodium-ion batteries.

1. Introduction

The development of large-scale energy storage systems (ESSs) has become one of the most important research areas in recent years.[1–3] Among several ESSs, lithium-ion batteries (LIBs) have been considered one of the most promising systems based on their high energy densities.[4,5] However, issues remain with LIBs as grid-scale ESSs, e.g. their increasing cost owing to limited global lithium resources to satisfy the high demand.[6] As such, sodium-ion systems are a less expensive and more abundant alternative for lithium-based ESSs and rechargeable batteries based on sodium have been studied in some depth in the quest to obtain cheaper and more sustainable ESSs.[7–11] Sodium-ion batteries (NIBs) are of particular interest for grid-scale ESSs for intermittent renewable energy.[12–15]

Considerable effort has been expended to obtain new sodium materials for NIBs that show high reversible capacity, rapid ion insertion-extraction and cycling stability.[16,17] Different compounds, such as metal oxides, polyanionic compounds and Prussian blue analogues, have demonstrated large sodium storage abilities for NIB applications. In particular, vanadium phosphate compounds such as $NaVOPO_4$, $NaVPO_4F$, $Na_3V_2(PO_4)_3$ and $Na_3V_2(PO_4)_2F_3$, show good electrochemical performance[18–21] and are promising cathode materials owing to their versatile structure, high stability, long-term cycling and low volumetric expansion during sodium insertion/extraction.

Recently, Kim and co-workers have explored the high-power cathode material $Na_4VO(PO_4)_2$ for NIB applications,[22] which has shown high redox potential and has an open framework for fast Na-ion diffusion. Deriouche et al. also examined the electrochemical properties of the $Na_4VO(PO_4)_2$ compound, demonstrating its high ionic conductivity and stability up to 700º C.[23] Previous works have demonstrated that cathode materials for NIBs with the V^{4+}/V^{5+} redox couple and the inductive effect of phosphorous ions, such as $Na_3V_2(PO_4)_3$ and $Na_3V_2(PO_4)_2F$, exhibit high operation voltages.[20,21,24,25]

In this study, we have investigated for the first time the electronic structure, ion diffusion and cation doping properties of the $Na_4VO(PO_4)_2$ compound by employing an effective combination of ab initio calculations and classical molecular dynamics simulation. We were able to reproduce the experimental structural parameters, before predicting the Na-ion diffusion mechanisms and voltage trends as a result of metal doping, where the doped structures show an increase in the cell voltage of up to 1.1 V *vs.* Na/Na⁺. From the molecular dynamic simulations, we have computed an activation energy of 0.49 eV for sodium diffusion. As such,

62 this material has a high Na-ion diffusion coefficient and low activation energy for Na-ion
63 migration, making it a promising cathode material for NIBs.

2. Methods

65 DFT calculations were performed using the Vienna Ab Initio Simulation Package (VASP).[26–
66 29] We used Projector-Augmented Wave (PAW) pseudopotentials[30,31] and the Perdew-Burke-
67 Ernzerhof exchange correlation functional revised for solids (PBEsol),[32] setting the kinetic
68 energy cut-off at 520 eV. A k-point grid of $5 \times 5 \times 5$ was used to converge the forces and
69 energies of the bulk material. The DFT+U methodology was applied to account for the d
70 orbitals of the metal atoms, with effective Hubbard values of $U_{eff} = U - J = 4.0, 3.3, 4.3, 3.9,$
71 6.0 and 4.2 eV (J = 1 eV) for V, Co, Fe, Mn, Ni and Ti, respectively.[21,33,34] These values are
72 consistent with previous studies of vanadium compounds as cathode materials.[21,33] A smaller
73 value of U_{eff} has been used for vanadium previously, leading to underestimated redox potentials
74 compared to experimental values. It was reported that a larger value of U_{eff} (4.0 eV) gives more
75 reliable agreement with experimental observations. In addition, Van der Waals contributions
76 via the DFT-D3 method of Grimme[35] were included, as these have been shown to influence
77 cell voltage calculations in some polyanionic systems.[36]

78 Previous computational studies on different metal oxide cathode materials have shown that
79 such methods are suitable to compute accurate cell voltage trends.[37] Furthermore, they have
80 also been shown to successfully determine transport and defect properties in Li-ion batteries.[38–
81 40] The cell voltage *vs*. Na/Na^{+} of the V^{4+}/V^{5+} redox couples were calculated using the following
82 equations:

$$V = E[Na_4VO(PO_4)_2] - E[Na_3VO(PO_4)_2] - \mu[Na] \qquad (1)$$

84 where $E[Na_4VO(PO_4)_2]$ and $E[Na_3VO(PO_4)_2]$ are the total energies of the $Na_4VO(PO_4)_2$ and
85 $Na_3VO(PO_4)_2$ compounds, respectively. All the compounds were geometry optimized to relax
86 their structures and obtain the most stable configuration. The chemical potential of sodium,
87 $\mu[Na]$, was calculated using metallic sodium, which is the standard practice for cell voltage
88 calculations. The MD simulations were performed using the LAMMPS code[41,42] and the
89 calculations were carried out on a large supercell made up of $7 \times 7 \times 7$ unit cells, comprising
90 15974 atoms. The initial configuration of the supercell contained 10% Na vacancies, plus
91 corresponding V^{5+} species, which were randomly distributed. Pre-equilibrium runs of 4 ps
92 using a time step of 2 fs within an NPT ensemble (constant number of particles, constant
93 pressure and constant temperature) were first used to obtain stable configurations. Simulation
94 runs were carried out using the NVT ensemble (constant number of particles, constant pressure

95 and constant temperature) and a time step of 1 fs for long runs of 10 ns, at temperatures in the

96 range of 300–1400 K. The interatomic potentials used in the MD calculations are listed in Table

97 SI1.

98 The mean squared displacement (MSD) of the Na cations, $[r(t)]^2$, for the $Na_4VO(PO_4)_2$

99 compound was computed to derive the diffusion coefficient (D_{Na}) using the equation:

$$\mathbf{D_{Na}} = \left(\frac{1}{6t}\right)\langle[\mathbf{r(t)}]^2\rangle \qquad (2)$$

101 where t is time and $<[r(t)]^2>$ is the MSD. A plot of the MSD *vs.* time at 300 and 600 K

102 for the $Na_4VO(PO_4)_2$ compound can be found in the Supporting Information as Figure

103 SI1.

3. Results and discussion

3.1 Structural analysis

106 The crystal structure, polymorphism and properties of $Na_4VO(PO_4)_2$ were first studied by Panin

107 et al.[43] The high temperature phase, α, crystallizes in the *Ibam* space group, whereas the low

108 temperature phase, β, crystallizes in the *Pbca* space group. It was shown that a reversible α−β

109 phase transition occurs at low temperature (~473 K). More recently, Lee and co-workers have

110 explored the application of the $Na_4VO(PO_4)_2$ compound as a cathode material for NIBs,[22]

111 where it showed high power capability owing to the high Na content, the numerous possible

112 Na diffusion paths, and the open framework structure.

113 The $Na_4VO(PO_4)_2$ compound has a similar structure to the high temperature modification of

114 the $Na_4TiO(PO_4)_2$ compound. The crystal structure of the $Na_4VO(PO_4)_2$ compound is depicted

115 in Figure 1a and consists of infinite VO_6 chains sharing common apical corners. The vanadium

116 octahedra are linked by two PO_4 tetrahedra resulting in a zigzag chain (Figure 1b). The

117 vanadium atoms are shifted from the equatorial plane of the octahedra towards one of the apical

118 oxygen atoms, forming short and long V-O bonds (1.75 and 2.04 Å, respectively), whereas all

119 equatorial V-O distances are similar (1.94-1.99 Å). This geometry shows the formation of the

120 characteristic vanadyl bond; these bonds have the same orientation along the *b*-axis of the

121 neighbouring chains, whereas they are oriented in an opposite way along the *a*-axis. The

122 phosphate groups are slightly distorted, showing P-O distances in the range of 1.52-1.56 Å.

123 The sodium atoms are located in the interstices between the chains and exist in four different

124 coordination arrangements (Figure 1c). The Na(1) atoms are coordinated to six oxygen atoms

125 forming a distorted octahedron with Na-O distances ranging from 2.30 to 2.46 Å. The Na(2)

126 atoms can be considered in a bicapped tetrahedron instead of an octahedron, showing Na-O

4

distances in the range 2.24-2.82 Å. The Na(3) atoms are located in a distorted tetrahedron and coordinate four oxygen atoms with Na-O distances ranging from 2.27 to 2.41 Å. Na(3) has three extra neighbouring oxygen atoms, although at a separation of more than 3Å. The Na(4) atoms are sited in the centre of a seven-atom polyhedron, which can be considered as a distorted trigonal antiprism and shows Na-O distances in the range 2.32-2.82 Å. A comparison of the experimental and computed cell parameters and averaged bond lengths can be found in Table **1** (the list with all the bond lengths is given in the Table SI2). The computed values are in good agreement with the experimental cell parameters and bond lengths.

a)

b)

c)

135
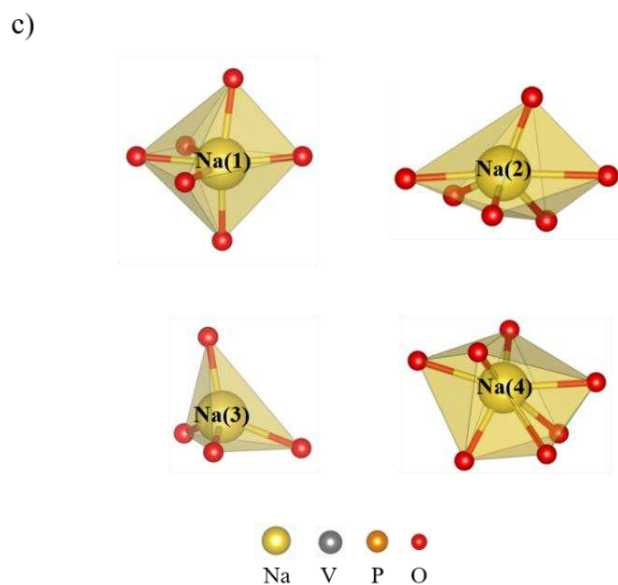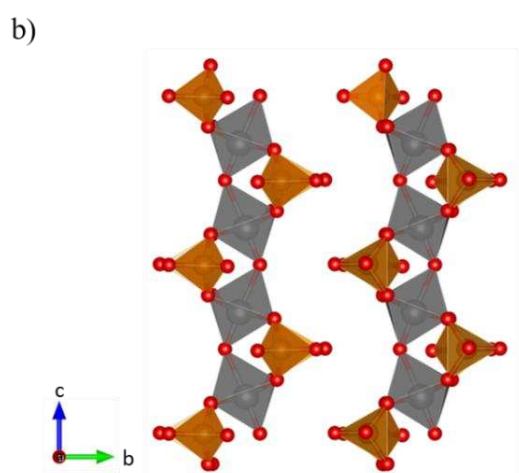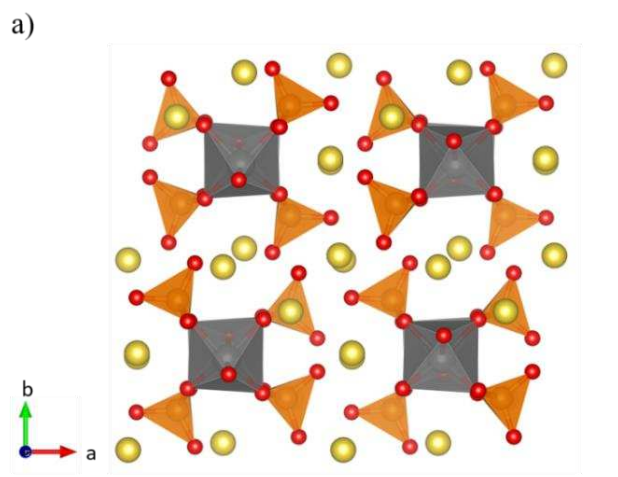
Figure 1. Polyhedral representation of (a) the $Na_4VO(PO_4)_2$ compound, (b) the vanadium chains
connected with the phosphate groups, where sodium atoms have been omitted for clarity, and
(c) the four different Na environments.

140   **Table 1.** Comparison of computed and experimental cell parameters and averaged bond lengths
141   of $Na_4VO(PO_4)_2$ compound (in Å).

	$Na_4VO(PO_4)_2$	
	Comp.	Exp.[a]
a	15.976	15.949
b	14.458	14.462
c	6.921	6.999
V-O	1.944	1.928
P-O	1.548	1.545
Na(1)-O	2.390	2.411
Na(2)-O	2.443	2.444
Na(3)-O	2.346	2.373
Na(4)-O	2.548	2.572
Symmetry	Orthorhombic	
Space group	*Pbca*	

142   [a] Ref. [22].

143   Polyhedral representations of the doped materials $Na_4V_{1-x}M_xO(PO_4)_2$ ($M = Al^{3+}$, Co^{2+}, Fe^{3+},
144   Mn^{4+}, Ni^{2+} or Ti^{4+}, and x = 0.25 or 0.50) are shown in Figure 2. In these structures, the dopant
145   atoms (M) have replaced either 25% or 50% of the V atoms. The crystal structures of the doped
146   compounds consist of infinite MO_6 chains sharing apical corners, where the MO_6 octahedra are
147   linked by two PO_4 tetrahedra resulting in a zigzag chain, as was also shown in Figure 1b. The
148   M atoms form short and long M-O bonds in the apical axis, like the V atoms in both the pristine
149   and doped materials. In the case of the Co-doped compound, the Co-O short and long bonds
150   are 1.74 and 2.02 Å, respectively; which are very similar to the V-O distances (1.75 and 2.04
151   Å, respectively). However, the short M-O distances in Al-, Fe-, Mn-, Ni- and Ti-doped
152   compounds are longer, ranging from 1.85 to 1.90 Å, although the long M-O distances retain

153 values between 2.01 and 2.07 Å. The P-O and Na-O distances in all doped materials are
154 comparable to those in the pristine material.
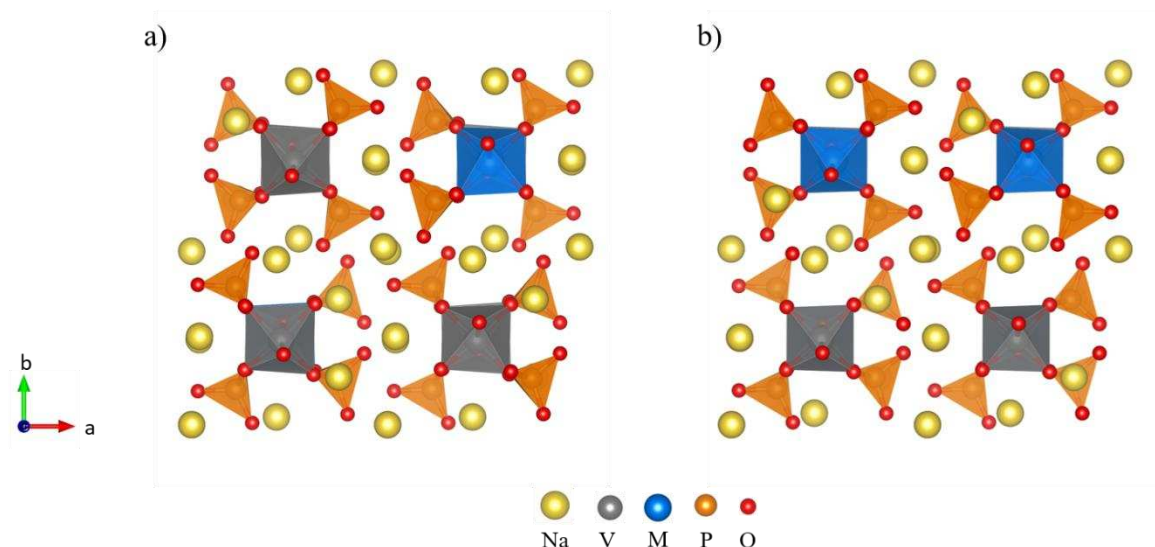
155
156 **Figure 2.** Polyhedral representation of the doped materials $Na_4V_{1-x}M_xO(PO_4)_2$, where M = Al^{3+}, Co^{2+},
157 Fe^{3+}, Mn^{4+}, Ni^{2+} or Ti^{4+}, and x = (a) 0.25 or (b) 0.50.

158 3.2 Cell voltage trend on cation doping
159 We have used the results from the DFT+U calculations to compute the cell voltages of the pure
160 and doped $Na_4VO(PO_4)_2$ compounds. To carry out the calculations, Na ions were removed
161 from the optimised structure and different vacancy positions were considered. The voltage was
162 then calculated, using Equation 1, for the lowest energy configuration. The computed voltage
163 of the $Na_4VO(PO_4)_2$ compound is 3.3 V *vs.* Na/Na^+, which is in good agreement with the
164 experimental value of ~3.5 V *vs.* Na/Na^+.
165 We have also investigated how doping on the vanadium site affects the cell voltage of the
166 $Na_4VO(PO_4)_2$ compound. The voltage trend of $Na_4V_{1-x}M_xO(PO_4)_2$ (M = Al^{3+}, Co^{2+}, Fe^{3+}, Mn^{4+},
167 Ni^{2+} or Ti^{4+}) *vs.* Na/Na^+ with varying x values (0, 0.25 or 0.50) is depicted in Figure 3. These
168 particular substitutional cations have already been used as doping agents in different vanadium
169 phosphate compounds, e.g. $NaVOPO_4$, $Li_3V_2(PO_4)_3$ and $Na_3V_2(PO_4)_3$.[44–52] The doped materials
170 showed higher capacity than the pristine compounds and the addition of the cation dopants
171 enhanced the electrochemical performance, the Li-ion and Na-ion diffusion, and the structural
172 stabilisation.
173 The computed cell voltage values of some of the doped structures were above the voltage
174 stability window for liquid Na-ion electrolytes (~3.5 V *vs.* Na/Na^+).[53] When x = 0.25, the Mn-
175 and Ti-doped structures are the only compounds whose voltage is within the voltage stability

176   window, whereas at x = 0.50, all the doped structures show computed voltages which are higher

177   than the electrochemical window for liquid electrolytes. We also observed that in the doped

178   materials, where the cation has an oxidation state different than 4+, some of the vanadium

179   atoms are oxidised to V^{5+} to compensate the charge. To summarise, the Mn^{4+} and Ti^{4+} cations

180   appear to be the most suitable dopants to increase the voltage of the $Na_4VO(PO_4)_2$ compound

181   within the operating voltage window of liquid electrolytes.

182
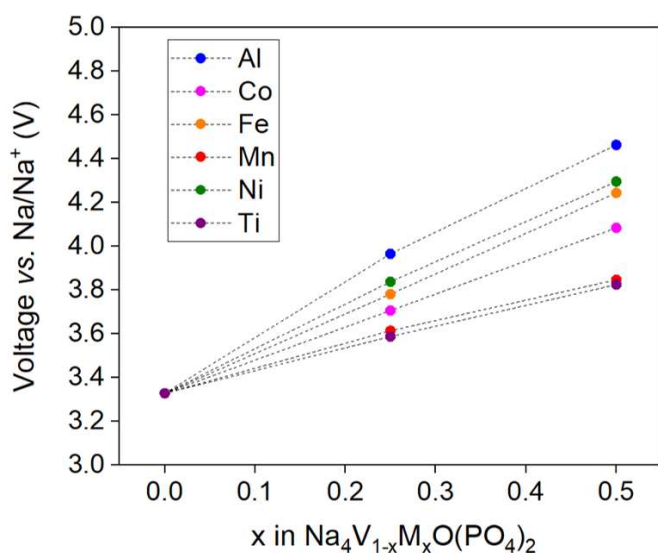
Figure 3. Cell voltage trend (*vs.* Na/Na⁺) of the $Na_4V_{1-x}M_xO(PO_4)_2$ compound as function of dopant
concentration (M = Al^{3+}, Co^{2+}, Fe^{3+}, Mn^{4+}, Ni^{2+} or Ti^{4+}) on the vanadium site.

185   3.3 Electronic analysis

186   The density of states (DOS) of the $Na_4VO(PO_4)_2$ compound is depicted in Figure 4. The

187   reported Curie-Weiss temperature is below 2 K, indicating a very weak magnetic interaction

188   between the vanadium spins, which behave almost like free spins.[43] This electronic

189   configuration cannot be computed, so we compared the energy of the ferromagnetic and

190   antiferromagnetic configurations. We found that the ferromagnetic solution, where all

191   vanadium spins are parallel, is the more stable configuration of the two. The valence band of

192   the DOS is described mainly by V 3d and O 2p electrons, whereas the conduction band is

193   mainly made up of V 3d electrons and the P atoms make only a relatively small contribution to

194   both valence and conduction bands. Below the Fermi level, from -0.3 to 0.0 eV, the total DOS

195   shows a contribution from the V 3d and the O 2p states, which corresponds to the short V=O

196   double bonds. The band gap of the studied compound is 1.8 eV, which is in good agreement

197   with previous GGA+U results of different vanadium phosphate compounds.[54]
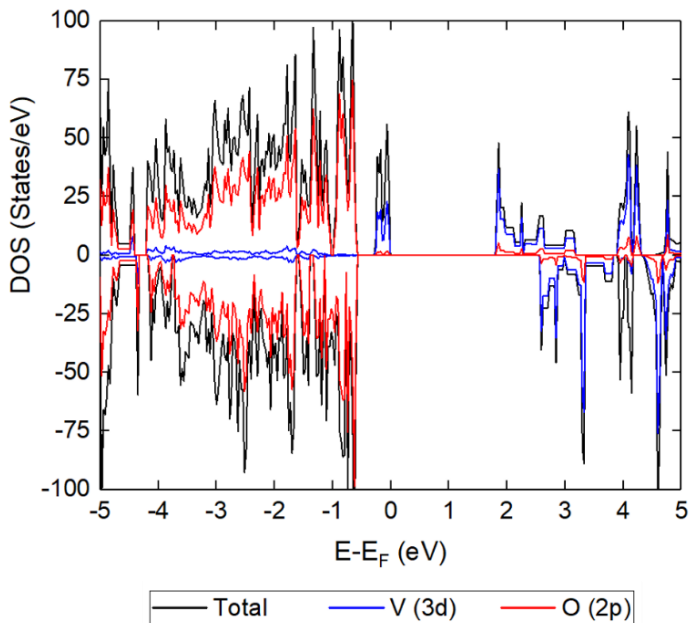
9

Figure 4. Density of States (DOS) of the $Na_4VO(PO_4)_2$ compound.

In general, the polyanionic compounds exhibit electronic properties of semiconductors or insulators. Metal-doping is a well-known strategy to change the electronic structure and improve ionic conductivity.[55–57] The electronic structure of the doped and pristine materials is very similar, with a small decrease of the band gap observed in all the doped compounds. Even though the decrease in the band gap is small, it can still facilitate electron conduction and thus accelerate the electron reaction kinetics. As a result, an improved electrochemical performance can be expected. The band gap reduction may be associated with the low electron affinity of the doped atoms compared to the V atom,[58] which causes an increase in the electronic conductivity.

3.3 Na-ion diffusion rates and pathways

MD simulations were performed over long timescales (10 ns) to examine long-range Na-ion transport. From the mean squared displacement (MSD) analysis, we observed that the diffusion takes place with equal probability in the three spatial directions. At 300 K, the diffusion coefficient (D_{Na}) of the $Na_4VO(PO_4)_2$ compound was calculated at 5.1×10^{-11} cm^2 s^{-1}. To the best of our knowledge, there are no experimental or computed values of this compound available in the literature for comparison. However, the computed D_{Na} is similar to those found in other vanadium phosphate cathode materials, e.g. $NaVOPO_4$ (10^{-11}-10^{-12} cm^2 s^{-1}),[59] and in other Na-ion cathode materials, such as Na_xCoO_2 (10^{-11} cm^2 s^{-1}),[60] Na_xMnO_2 (10^{-11} cm^2 s^{-1})[61]

219 and Na_2CoSiO_4 (10^{-12} cm^2 s^{-1}).[62] Using the Nernst-Einstein equation we have converted the
220 diffusion coefficient to conductivity which was found to be equal to 7.5×10^{-3} S cm^{-1}. This
221 value obtained from our calculations is very similar to the experimental value of 10^{-4} S cm^{-1}.
222 The MD calculations were performed at different temperatures between 300 and 1400 K,
223 covering a larger range than only the typical NIB operating temperatures. The computed
224 diffusion coefficients at different temperatures can be used to estimate activation energies from
225 an Arrhenius plot (ln D_{Na} vs. 1/T), as shown in Figure 5.

226
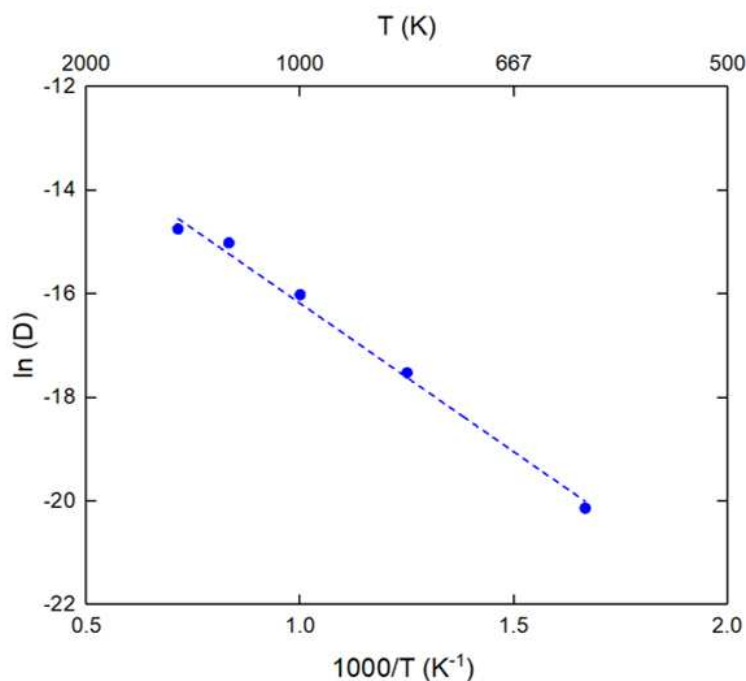
Figure 5. Arrhenius plot of Na-ion diffusion coefficients vs. temperature for the $Na_4VO(PO_4)_2$
228 compound.

229 The activation energy for the onset of diffusion of the sodium ion in the $Na_4VO(PO_4)_2$
230 compound was calculated at 0.49 eV, which is similar to the values of other vanadium
231 phosphate compounds. Diffusion trajectories of Na ions are visualised in Figure 6 by plotting
232 accumulated Na-ion densities, indicating the most frequently crossed sites during the MD
233 simulation. As derived from the MSD analysis, we observed from the Na densities that the
234 diffusion takes place along 3D channels. These results confirm that Na ions are highly mobile
235 in the $VO(PO_4)_2$ framework, with all the Na sites involved in the diffusion.

Na   V   P   O
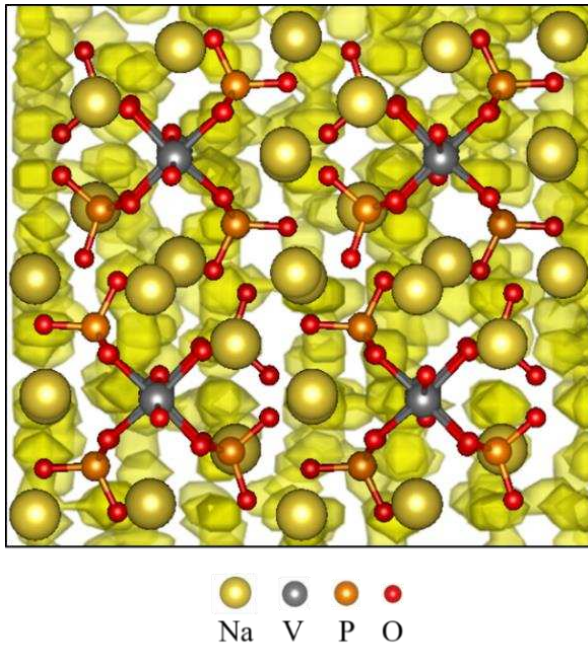
Figure 6. Na density plot from MD simulations at 700 K showing the Na diffusion pathways of the Na$_4$VO(PO$_4$)$_2$ compound. Na-ion density is plotted in yellow.

4. Conclusions

The sodium vanadyl phosphate Na$_4$VO(PO$_4$)$_2$ is one of the most promising cathode materials for sodium-ion batteries because of its good electrochemical performance. Here, we have studied the electronic structure, diffusion and cation doping properties of the Na$_4$VO(PO$_4$)$_2$ compound. Our work shows good reproduction of the observed experimental structure and it also reveals key atomistic insights into the ionic transport properties. From the MD simulations, we derived an Na ion activation energy of 0.49 eV and a diffusion coefficient at 300 K of D$_{Na}$ = 5.1×10^{-11} cm^2 s^{-1}. Analysis of the migration pathways shows that the Na-ion diffusion in the Na$_4$VO(PO$_4$)$_2$ compound takes place along 3-dimensional channels. The DFT-computed cell voltage of 3.3 V *vs.* Na/Na$^+$ agrees well with the reported electrochemical data, whereas cation doping (Al^{3+}, Co^{2+}, Fe^{3+}, Mn^{4+}, Ni^{2+} and Ti^{4+}) at the vanadium site is predicted to increase the cell voltage. The Mn- and Ti-doped materials show an increase of the cell voltage within the electrochemical stability window of current liquid electrolytes.

Overall, the fundamental insights presented in this work will help us understand the ionic transport properties of phosphate cathode materials for sodium-ion batteries.

Author information

Corresponding authors:

apariciosanchezp@cardiff.ac.uk

257 deleeuwn@cardiff.ac.uk

258 Notes:

References

267 1   K. C. Divya and J. Østergaard, *Electr. Power Syst. Res.*, 2009, **79**, 511–520.

268 2   B. Dunn, H. Kamath and J.-M. Tarascon, *Science (80-.).*, 2011, **334**, 928–935.

269 3   S. Hameer and J. L. van Niekerk, *Int. J. Energy Res.*, 2015, **39**, 1179–1195.

270 4   J.-M. Tarascon and M. Armand, *Nature*, 2001, **414**, 359–367.

271 5   M. Armand and J.-M. Tarascon, *Nature*, 2008, **451**, 652–657.

272 6   H. Vikström, S. Davidsson and M. Höök, *Appl. Energy*, 2013, **110**, 252–266.

273 7   S. W. Kim, D. H. Seo, X. Ma, G. Ceder and K. Kang, *Adv. Energy Mater.*, 2012, **2**,
274   710–721.

275 8   S. Y. Hong, Y. Kim, Y. Park, A. Choi, N.-S. Choi and K. T. Lee, *Energy Environ. Sci.*,
276   2013, **6**, 2067–2081.

277 9   H. Pan, Y.-S. Hu and L. Chen, *Energy Environ. Sci.*, 2013, **6**, 2338–2360.

278 10   N. Yabuuchi, K. Kubota, M. Dahbi and S. Komaba, *Chem. Rev.*, 2014, **114**, 11636–
279   11682.

280 11   H. Kim, H. Kim, Z. Ding, M. H. Lee, K. Lim, G. Yoon and K. Kang, *Adv. Energy
281   Mater.*, 2016, **6**, 1600943.

282 12   C. Fang, Y. Huang, W. Zhang, J. Han, Z. Deng, Y. Cao and H. Yang, *Adv. Energy
283   Mater.*, 2016, **6**, 1501727.

284   13   J.-Y. Hwang, S.-T. Myung and Y.-K. Sun, *Chem. Soc. Rev.*, 2017, **46**, 3529–3614.

285   14   D. Kundu, E. Talaie, V. Duffort and L. F. Nazar, *Angew. Chemie Int. Ed.*, 2015, **54**,
286   3432–3448.

287   15   Q. Ni, Y. Bai, F. Wu and C. Wu, *Adv. Sci.*, 2017, **4**, 1600275.

288   16   N. Yabuuchi, K. Kubota, M. Dahbi and S. Komaba, *Chem. Rev.*, 2014, **114**, 11636–
289   11682.

290   17   M. H. Han, E. Gonzalo, G. Singh and T. Rojo, *Energy Environ. Sci.*, 2015, **8**, 81–102.

291   18   J. Song, M. Xu, L. Wang and J. B. Goodenough, *Chem. Commun.*, 2013, **49**, 5280–
292   5282.

293   19   J. Barker, M. Y. Saidi and J. L. Swoyer, *Electrochem. Solid-State Lett.*, 2003, **6**, A1–
294   A4.

295   20   S. Y. Lim, H. Kim, R. A. Shakoor, Y. Jung and J. W. Choi, *J. Electrochem. Soc.*, 2012,
296   **159**, A1393–A1397.

297   21   R. A. Shakoor, D.-H. Seo, H. Kim, Y.-U. Park, J. Kim, S.-W. Kim, H. Gwon, S. Lee
298   and K. Kang, *J. Mater. Chem.*, 2012, **22**, 20535–20541.

299   22   J. Kim, H. Kim and S. Lee, *Chem. Mater.*, 2017, **29**, 3363–3366.

300   23   W. Deriouche, E. Anger, M. Freire, A. Maignan, N. Amdouni and V. Pralong, *Solid*
301   *State Sci.*, 2017, **72**, 124–129.

302   24   Z. Jian, W. Han, X. Lu, H. Yang, Y. S. Hu, J. Zhou, Z. Zhou, J. Li, W. Chen, D. Chen
303   and L. Chen, *Adv. Energy Mater.*, 2013, **3**, 156–160.

304   25   Y. H. Jung, C. H. Lim and D. K. Kim, *J. Mater. Chem. A*, 2013, **1**, 11350–11354.

305   26   G. Kresse and J. Hafner, *Phys. Rev. B*, 1993, **47**, 558–561.

306   27   G. Kresse and J. Hafner, *Phys. Rev. B*, 1994, **49**, 14251–14269.

307   28   G. Kresse and J. Furthmüller, *Comput. Mater. Sci.*, 1996, **6**, 15–50.

308   29   G. Kresse and J. Furthmüller, *Phys. Rev. B*, 1996, **54**, 11169–11186.

309   30   P. E. Blöchl, *Phys. Rev. B*, 1994, **50**, 17953–17979.

310   31   G. Kresse and D. Joubert, *Phys. Rev. B*, 1999, **59**, 1758–1775.

311 32 J. P. Perdew, A. Ruzsinszky, G. I. Csonka, O. A. Vydrov, G. E. Scuseria, L. A.
312   Constantin, X. Zhou and K. Burke, *Phys. Rev. Lett.*, 2008, **100**, 136406.

313 33 A. A. Tsirlin, R. Nath, A. M. Abakumov, Y. Furukawa, D. C. Johnston, M. Hemmida,
314   H.-A. Krug von Nidda, A. Loidl, C. Geibel and H. Rosner, *Phys. Rev. B*, 2011, **84**,
315   14429.

316 34 J. Heath, H. Chen and M. S. Islam, *J. Mater. Chem. A*, 2017, **5**, 13161–13167.

317 35 S. Grimme, J. Antony, S. Ehrlich and H. Krieg, *J. Chem. Phys.*, 2010, **132**, 154104.

318 36 C. Eames, J. M. Clark, G. Rousse, J. M. Tarascon and M. S. Islam, *Chem. Mater.*,
319   2014, **26**, 3672–3678.

320 37 M. S. Islam and C. A. J. Fisher, *Chem. Soc. Rev.*, 2014, **43**, 185–204.

321 38 J. M. Clark, C. Eames, M. Reynaud, G. Rousse, J.-N. Chotard, J.-M. Tarascon and M.
322   S. Islam, *J. Mater. Chem. A*, 2014, **2**, 7446–7453.

323 39 J. Roos, C. Eames, S. M. Wood, A. Whiteside and M. S. Islam, *Phys. Chem. Chem.*
324   *Phys.*, 2015, **17**, 22259–22265.

325 40 C. Tealdi, J. Heath and M. S. Islam, *J. Mater. Chem. A*, 2016, **4**, 6998–7004.

326 41 LAMMPS website, http://lammps.sandia.gov.

327 42 S. Plimpton, *J. Comput. Phys.*, 1995, **117**, 1–19.

328 43 R. V. Panin, R. V. Shpanchenko, A. V. Mironov, Y. A. Velikodny, E. V. Antipov, V.
329   A. Tarnopolsky, A. B. Yaroslavtsev, E. E. Kaul, C. Geibel and J. Hadermann, *Chem.*
330   *Mater.*, 2004, **16**, 1048–1055.

331 44 M. Ren, Z. Zhou, Y. Li, X. P. Gao and J. Yan, *J. Power Sources*, 2006, **162**, 1357–
332   1362.

333 45 Q. Kuang, Y. Zhao, X. An, J. Liu, Y. Dong and L. Chen, *Electrochim. Acta*, 2010, **55**,
334   1575–1581.

335 46 C. Deng, S. Zhang, S. Y. Yang, Y. Gao, B. Wu, L. Ma, B. L. Fu, Q. Wu and F. L. Liu,
336   *J. Phys. Chem. C*, 2011, **115**, 15048–15056.

337 47 Y. Zhang, Q. Huo, Y. Lv, L. Wang, A. Zhang, Y. Song, G. Li, H. Gao, T. Xia and H.
338   Dong, *J. Alloys Compd.*, 2012, **542**, 187–191.

339   48   L.-L. Zhang, G. Liang, G. Peng, Y.-H. Huang, L. Wang, L. Qie, M. C. Croft, A.
340   Ignatov and J. B. Goodenough, *J. Electrochem. Soc.*, 2012, **159**, A1573–A1578.

341   49   D. Tao, S. Wang, Y. Liu, Y. Dai, J. Yu and X. Lei, *Ionics (Kiel).*, 2015, **21**, 1201–
342   1239.

343   50   C. Lai, Z. Chen, H. Zhou, Y. Lu and H. Li, *J. Mater. Sci.*, 2015, **50**, 3075–3082.

344   51   H.-B. Sun, L.-L. Zhang, X.-L. Yang, G. Liang and Z. Li, *Dalt. Trans.*, 2016, **45**,
345   15317–15325.

346   52   B. Zhang, H. Chen, H. Tong, X. Wang, J. Zheng, W. Yu, J. Zhang, J. Li and W.
347   Zhang, *J. Alloys Compd.*, 2017, **728**, 976–983.

348   53   A. Ponrouch, R. Dedryvère, D. Monti, A. E. Demet, J. M. Ateba Mba, L. Croguennec,
349   C. Masquelier, P. Johansson and M. R. Palacín, *Energy Environ. Sci.*, 2013, **6**, 2361–
350   2369.

351   54   W. Sun and J. Du, *Comput. Mater. Sci.*, 2017, **126**, 326–335.

352   55   M. J. Aragón, P. Lavela, R. Alcántara and J. L. Tirado, *Electrochim. Acta*, 2015, **180**,
353   824–830.

354   56   X. Zhao, G. Liang, H. Liu and Y. Liu, *RSC Adv.*, 2018, **8**, 4142–4152.

355   57   D. Jin, H. Qiu, F. Du, Y. Wei and X. Meng, *Solid State Sci.*, 2019, **93**, 62–69.

356   58   L. Zhao, H. Zhao, Z. Du, N. Chen, X. Chang, Z. Zhang, F. Gao, A. Trenczek-Zajac
357   and K. Świerczek, *Electrochim. Acta*, 2018, **282**, 510–519.

358   59   P. A. Aparicio, J. A. Dawson, M. S. Islam and N. H. de Leeuw, *J. Phys. Chem. C*,
359   2018, **122**, 25829–25836.

360   60   T. Shibata, W. Kobayashi and Y. Moritomo, *Appl. Phys. Express*, 2013, **6**, 97101.

361   61   T. Shibata, W. Kobayashi and Y. Moritomo, *Appl. Phys. Express*, 2014, **7**, 67101.

362   62   J. C. Treacher, S. M. Wood, M. S. Islam and E. Kendrick, *Phys. Chem. Chem. Phys.*,
363   2016, **18**, 32744–32752.

364